

## Epoxidized natural rubber toughened poly(lactic acid)/halloysite nanocomposites with high activation energy of water diffusion

Wei Ling Tham,<sup>1</sup> Beng Teik Poh,<sup>2</sup> Zainal Arifin Mohd Ishak,<sup>1</sup> Wen Shyang Chow<sup>1</sup>

<sup>1</sup>School of Materials and Mineral Resources Engineering, Universiti Sains Malaysia, Penang 14300, Malaysia

<sup>2</sup>School of Industrial Technology, Universiti Sains Malaysia, Penang 11800, Malaysia

Correspondence to: W.S. Chow (E-mail:shyang@usm.my)

**ABSTRACT:** Poly(lactic acid)/halloysite nanotube (PLA/HNT) nanocomposites were prepared using melt compounding followed by compression molding. Epoxidized natural rubber (ENR) was used to toughen the PLA nanocomposites. The properties of PLA/HNT nanocomposites were characterized by impact tests, thermal analysis (DSC), morphological analysis (FESEM, TEM), and Fourier transform infrared spectroscopy (FTIR). Water absorption tests were performed at three immersion temperature (30, 40, 50°C). The maximum water absorption ( $M_m$ ), diffusion coefficient ( $D$ ), and the activation energy of water diffusion ( $E_a$ ) were determined. The impact strength of PLA/HNT6 nanocomposites was increased significantly to ~296% by the addition of 15 wt % ENR. The incorporation of HNT and ENR increase its nucleation effect and assist in the crystallization process of PLA. The HNT has good affinity with PLA and ENR, which was revealed by TEM and FTIR. The  $M_m$  of PLA was increased in the presence of HNT and ENR. Nevertheless, the  $D$  value and the  $E_a$  of the PLA nanocomposites were found to be affected by the HNT and ENR contents. © 2015 Wiley Periodicals, Inc. *J. Appl. Polym. Sci.* **2016**, *133*, 42850.

**KEYWORDS:** biodegradable; composites; differential scanning calorimetry (DSC); polyesters

Received 1 July 2015; accepted 18 August 2015

DOI: 10.1002/app.42850

### INTRODUCTION

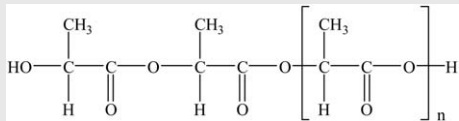
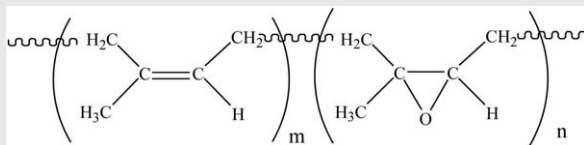
Polymer nanocomposites are produced by incorporating nanomaterials such as nanofillers, nanoparticles, nanoscale building block, or nanoreinforcement that have one or more dimensional silicate gallery on the nanometer scale (<100 nm) into a polymer matrix. Polymer nanocomposites have enhanced stiffness, strength, toughness, thermal stability, barrier properties, and flame retardancy compared to pure polymer matrix. It was attributed to the nanosize dispersion of nanofiller in the polymer, high aspect ratio of nanofiller, and interfacial interaction between nanofiller and polymers.<sup>1</sup>

Recent developments pertaining to the economical manufacturing of lactic acid from renewable agricultural resources (e.g., corn, potato, sugar beet, sugar cane) have made poly(lactic acid) (PLA) one of the most important biodegradable polymers.<sup>2–4</sup> PLA offers good mechanical properties (i.e., high strength and modulus), a high degree of transparency, facile processability, good biocompatibility, and excellent biodegradability. The PLA has the potential to replace engineering plastic such as polyamide (PA) and polycarbonate (PC) due to its high mechanical properties being close to some engineering polymers. However, there is a challenge for PLA to replace engineering plastics because of its low thermal stability, high brittleness,

low elongation at break, and high cost limits its application.<sup>5,6</sup> Incorporating micro- or nanofillers into PLA is a promising way in enhancing the mechanical properties, thermal properties, gas barrier, and crystallization behaviour of PLA.<sup>7</sup> Recently, the HNT has been used as a reinforcing filler and nucleating agent for various polymer, such as poly(propylene) (PP), vinyl ester, polyamide (PA), poly(vinyl chloride) (PVC), and epoxy for enhancing the mechanical, thermal, crystallization, fire, and other specific properties.<sup>7</sup>

To overcome the brittleness of polymer, the addition of impact modifier or elastomer in polymer composite could be a good strategy.<sup>8,9</sup> A balance property between stiffness and toughness of polymer has been received increasing interest among researchers. Epoxidized natural rubber (ENR) has been used as polymeric compatibilizer,<sup>10</sup> interfacial modifier,<sup>11</sup> and toughening agent.<sup>12</sup> Epoxidized natural rubber (ENR) is a chemically modified form of the *cis*-1,4-polyisoprene rubber, whereby the unsaturation of hydrocarbon is replacing with epoxide groups that are randomly distributed along the polymer chain.<sup>13</sup> Epoxidation of natural rubber raises the glass transition temperature ( $T_g$ ) by ~1°C for every mole % epoxidation. This increase in glass transition temperature of ENR increases damping and reduces gas permeability. The presence of epoxide group in

**Table I.** Chemical Structure of Materials

| Materials                       | Chemical structure   |
|---------------------------------|--|
| Poly(lactic acid) (PLA)         |  |
| Halloysite nanotube (HNT)       | $\text{Al}_2(\text{OH})_4\text{Si}_2\text{O}_5(2\text{H}_2\text{O})$               |
| Epoxidized natural rubber (ENR) |  |

ENR introduced polarity and made the rubber more versatile for rubber–rubber or rubber–plastic blending.<sup>14</sup>

In this article, the effects of ENR on the impact properties, thermal properties, and morphology of PLA/HNT nanocomposites are discussed. The interactions between PLA, HNT, and ENR were confirmed by TEM and FTIR. Unlike biodegradable PLA used for packaging and agriculture, the PLA used in engineering applications demand higher durability and longer service duration. Despite possessing good mechanical properties, the durability PLA/HNT nanocomposites must be sufficiently high in order to be applied in harsh environments during their service life. Therefore, the effects of HNT and ENR content on the water absorption kinetic of PLA at different immersion temperatures (i.e., 30, 40, and 50°C) were investigated. The diffusion coefficient ( $D$ ) and activation energy of water diffusion ( $E_a$ ) of PLA nanocomposites were analyzed.

## EXPERIMENTAL

### Materials

PLA (Ingeo™ 3051D, NatureWorks LLC®, USA) was selected for use in this study. The specific gravity and melt flow index of PLA were 1.25 and 25 g 10<sup>-1</sup> min<sup>-1</sup>, respectively (2.16 kg load, 210°C). The halloysite nanotube (HNT) was supplied by Sigma–Aldrich (USA). The diameter of the HNT was in the range of 30–70 nm with a length of 1–3 μm. Epoxidized natural rubber (ENR 50) containing 50 mol % of epoxidation was supplied by the Rubber Research Institute of Malaysia. The average molecular weight ( $M_n$ ) of ENR 50 is 8 × 10<sup>4</sup> kg mol<sup>-1</sup>. No commercial modifier was added to the rubber. Table I shows the materials used in the research and chemical structure of the materials.

### Sample Preparation

Melt compounding was carried out using a Haake Polydrive R600 internal mixer (Thermo Electron Scientific, Germany) at 180°C for 10 min. The rotor speed was set at 50 rpm. Prior to compounding, PLA and HNT were dehumidified in a vacuum oven at 60°C for 24 h. The compression molding was performed at 185°C using a hot press machine (Gotech testing machines, Taiwan). The preheating, compression molding, and cooling times were 7, 3, and 3 min, respectively. Table II shows the

material designations and compositions of the PLA/HNT nanocomposites.

### Sample Characterization

**Impact Test.** The Charpy impact strength of the samples was determined according to ASTM D6110 by using a pendulum impact machine (model 5101, Zwick, Germany). The dimension of sample was 65 mm × 13 mm × 3 mm (length × width × thickness). The testing was performed with pendulum of 7.5 J with a velocity of 3.54 m s<sup>-1</sup>.

**Differential Scanning Calorimetry (DSC).** The melting and crystallization behaviour of the composites were scanned under nitrogen atmosphere by DSC 1 (Mettler Toledo STAR<sup>c</sup>, USA) using ~10 mg samples sealed in aluminium pans. The specimens were scanned from 30 to 200°C at a heating rate of 10°C min<sup>-1</sup>. The glass transition temperature ( $T_g$ ), melting temperature ( $T_m$ ), cold crystallization temperature ( $T_{cc}$ ), and degree of crystallinity ( $\chi_c$ ) of the PLA nanocomposites were determined. The degree of crystallinity ( $\chi_c$ ) of PLA nanocomposites was evaluated according to eq. (1).

$$\chi_c = [\Delta H_m / (\Delta H_f \cdot w_{\text{PLA}})] \times 100\% \quad (1)$$

where  $\Delta H_m$  is the enthalpy of melting;  $\Delta H_f$  is the enthalpy for 100% crystalline PLA, and  $w_{\text{PLA}}$  is the net weight fraction of the PLA. The heat of fusion for 100% crystalline PLA is ~93.6 J g<sup>-1</sup>.<sup>15</sup>

**Fourier Transform Infrared Spectroscopy (FTIR).** FTIR spectrophotometer (Perkin Elmer Spectrum One, UK) was used to characterize the functional group of PLA/HNT nanocomposites

**Table II.** Materials Designations and Compositions of PLA Nanocomposites

| Materials designation | PLA/wt % | HNT/wt % | ENR/wt % |
|-----------------------|----------|----------|----------|
| PLA                   | 100      | -        | -        |
| PLA/HNT6              | 94       | 6        | -        |
| PLA/HNT6/ENR5         | 89       | 6        | 5        |
| PLA/HNT6/ENR10        | 84       | 6        | 10       |
| PLA/HNT6/ENR15        | 79       | 6        | 15       |
| PLA/HNT6/ENR20        | 74       | 6        | 20       |

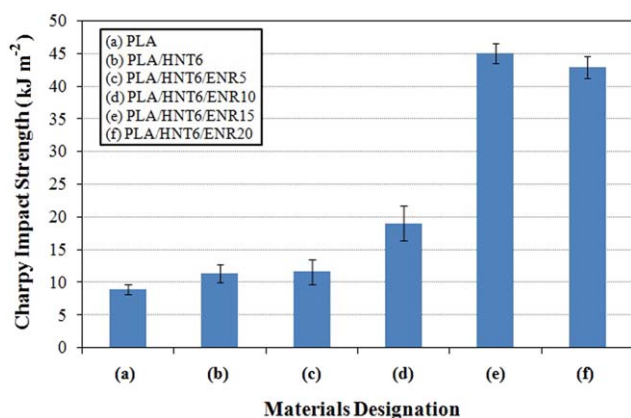


**Figure 1.** Effect of ENR on the impact strength of PLA/HNT6 nanocomposites. [Color figure can be viewed in the online issue, which is available at [wileyonlinelibrary.com](http://wileyonlinelibrary.com).]

and carbonyl index (CI) determination. FTIR spectra were determined from 400 to 4000  $\text{cm}^{-1}$  by using IR Spectroscopy Spectrum Version 5.0.1 software at 40 scans with a resolution of 4  $\text{cm}^{-1}$ .

**Field Emission Scanning Electron Microscope (FESEM).** The fracture surfaces of selected PLA composites were investigated in a field emission scanning electron microscope (FESEM, Zeiss Supra 35VP, Germany) at an acceleration voltage of 5 kV. The specimen surfaces were gold coated to avoid electrostatic charging during examination.

**Transmission Electron Microscopy (TEM).** PLA specimens ( $\sim 50$  nm) were prepared using a PT-PC PowerTome ultramicrotome (Boeckeler Instruments, AZ) with a diatome diamond knife. TEM viewing was then performed using a Zeiss Libra 120 Plus energy filtering transmission electron microscope (Carl Zeiss, Germany) operating at an accelerating voltage of 120 kV.

**Water Absorption Tests.** The specimens (dimension: 65 mm  $\times$  13 mm  $\times$  3 mm) were dried at 50°C in vacuum oven until a constant weight was attained. Then, they were immersed in water in a thermostated stainless steel water bath at 30, 40, and 50°C. Weight changes were recorded by periodic removal of the specimens from the water bath and weighing on a balance with a precision of 1 mg. The percentage change at any time  $t$ , ( $M_t$ ) as a result of water absorption was determined by eq. (2):

$$M_t = [(W_w - W_d) / W_d] \times 100\% \quad (2)$$

where  $W_d$  and  $W_w$  denote the weight of dry material (the initial weight) and weight of materials after exposure to water absorption, respectively. The percentage at maximum water absorption ( $M_m$ ) was calculated as the average value of several consecutive measurements that showed no appreciable additional absorption. The weight gain, resulting from moisture absorption, can be expressed in terms of two parameters, the diffusion coefficient ( $D$ ) and the  $M_m$ , using eq. (3).

$$M_t / M_m = 1 - (8 / \pi^2) \exp[-(Dt/h^2)\pi^2] \quad (3)$$

where  $h$  is the thickness of the specimens. The  $D$  value can be calculated after rearranging eq. (3) into eq. (4), as follows:

$$D = [\pi h^2 (M_2 - M_1)^2] / [16 M_m^2 (t_2^{1/2} - t_1^{1/2})^2] \quad (4)$$

where  $(M_2 - M_1)^2 / (t_2^{1/2} - t_1^{1/2})^2$  is the initial linear portion of the slope of  $M_t$  versus  $t^{1/2}$ .

The activation energies of water diffusion for the PLA nanocomposites were determined by using Arrhenius Equation [see eq. (5)].

$$D = D_0 \exp[-(E_a / RT)] \quad (5)$$

where  $D$  is the diffusion coefficient of the sample;  $D_0$  is the initial diffusion coefficient of the sample;  $E_a$  is the activation energy of water diffusion;  $R$  is gas constant (8.314 J  $\text{K}^{-1}$   $\text{mol}^{-1}$ ) and  $T$  is the temperature. By plotting the graph of  $\ln(D)$  of the samples versus reciprocal of temperature,  $1/T$ , activation energy of the water diffusion can be obtained [c.f., eq. (6)].

$$\ln D = -(E_a / RT) + \ln D_0 \quad (6)$$

## RESULTS AND DISCUSSION

### Impact Test

Figure 1 shows that the impact strength of PLA was increased to 11.4  $\text{kJ m}^{-2}$  with the addition of 6 wt % HNT. This was attributed to the well-dispersed and nano-particle sizes of HNT, creating the voids that could act as initiation sites at the interface of PLA and HNT. This leads to the plastic deformation in the PLA matrix around the neighbouring HNT. As a result, a substantial amount of energy was dissipated due to several localised energy dissipating processes induced by HNT. This finding was reported by Zuiderduin *et al.*<sup>16</sup> in PP/ $\text{CaCO}_3$  nanocomposites and Lin *et al.*<sup>17</sup> in PS/HNT nanocomposites. It is worth mentioning that the incorporation of 15 wt % ENR increased the impact strength dramatically to  $\sim 296\%$  in PLA/HNT6 nanocomposite. It can be suggested that the addition of ENR into PLA nanocomposites can absorb much more energy when load is applied and remarkably improve the impact strength of PLA/HNT. This was attributed to the good interaction between PLA, HNT, and ENR, which may reduce their interfacial energy in the interfacial region. Thus, create a finer dispersion in improving stress transfer, which in turn increases the PLA impact strength. Therefore, the ENR could absorb high

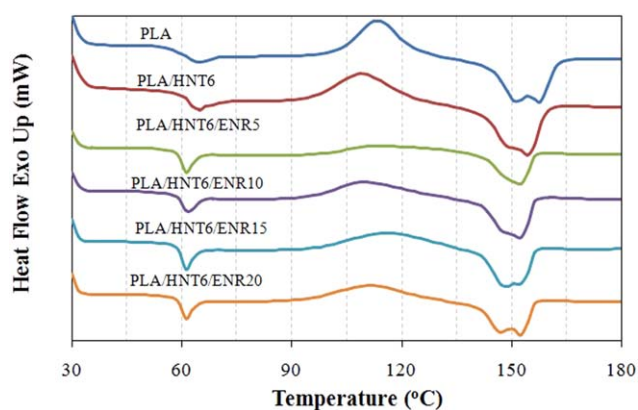


**Figure 2.** DSC heating curve of PLA and PLA/HNT6 nanocomposites (with and without ENR). [Color figure can be viewed in the online issue, which is available at [wileyonlinelibrary.com](http://wileyonlinelibrary.com).]

**Table III.** Thermal Characteristics of PLA and PLA/HNT6 Nanocomposites (With and without ENR) Recorded from DSC

| Materials designation | $T_g$ (°C) | $T_{cc}$ (°C) | $T_{m,1}$ (°C) | $T_{m,2}$ (°C) | $T_c$ (°C) | $\chi_c$ (%) |
|-----------------------|------------|---------------|----------------|----------------|------------|--------------|
| PLA                   | 58.7       | 113.5         | 150.7          | 157.5          | -          | 29.9         |
| PLA/HNT6              | 60.3       | 109.0         | 150.7          | 154.3          | -          | 31.3         |
| PLA/HNT6/ENR5         | 58.6       | 112.3         | -              | 152.3          | -          | 16.5         |
| PLA/HNT6/ENR10        | 60.7       | 110.1         | 148.2          | 152.5          | -          | 25.8         |
| PLA/HNT6/ENR15        | 60.2       | 116.0         | 148.6          | 152.1          | -          | 25.0         |
| PLA/HNT6/ENR20        | 60.1       | 111.3         | 147.5          | 152.5          | -          | 33.2         |

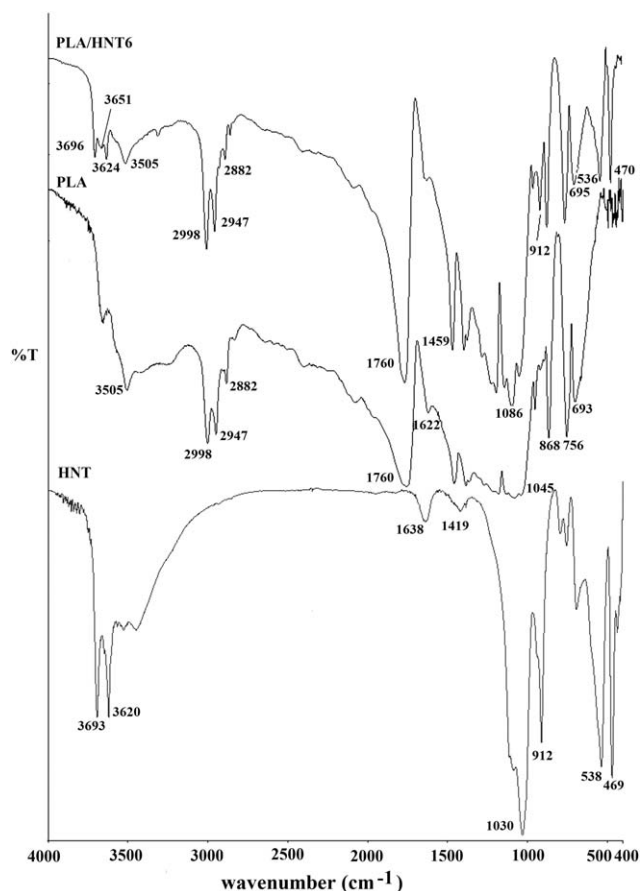
amounts of energy when the load transfers from ENR to PLA and create multiple crack propagation in the vicinity of ENR particles at a high impact speed. Consequently, the formation of multiple crack propagation gives rise to the overall deformation toughness of PLA nanocomposite system in dissipating higher energy. The cavitation or debonding of rubber particles play an important role in increasing the toughness of polymer due to energy dissipation.<sup>18,19</sup>

#### Differential Scanning Calorimetry (DSC)

Figure 2 shows the DSC heating curve of PLA and PLA/HNT6 nanocomposites (with and without ENR) which the data is summarized in Table III. From Table III, it can be noted that the  $T_g$  of PLA nanocomposite with the addition of ENR occurs at the same temperature around 60°C. It is indicated that the addition of ENR did not have obvious influence on the  $T_g$  of PLA. It can be seen that the neat PLA displayed two melting peaks i.e., 150.7°C ( $T_{m,1}$ ) and 157.5°C ( $T_{m,2}$ ). The PLA/HNT6 nanocomposites also occurred at two melting temperatures of 150.7 and 154.3°C. Double melting endotherms can be attributed to the melt recrystallization mechanism of PLA, which is originated from PLA crystal growth. The less perfect crystals ( $\alpha'$ -form crystal) of PLA have sufficient time to melt and reorganize into perfect crystals ( $\alpha$ -form crystals) before giving a second endotherm at higher temperature.<sup>20–22</sup> The melting peaks at  $T_{m,1}$  and  $T_{m,2}$  of PLA/HNT nanocomposites slightly shifted to a low temperature with the incorporation of ENR. The melting peak at relatively lower temperature ( $T_{m,1} = 147–148^\circ\text{C}$ ) becomes more obvious with the increasing of ENR content, whereas the second melting peak ( $T_{m,2}$ ) at relatively higher temperature is maintained at 152°C. The presence of ENR may retard the formation of perfect crystallites of PLA, thus, double-melting peak can be associated with formation of different lamellae thickness and the melt-recrystallization mechanism.<sup>23</sup>

The addition of 6 wt % of HNT slightly shifted the cold crystallization temperature ( $T_{cc}$ ) of PLA to a lower temperature from 113.5 to 109.0°C. Also, the percentage of  $\chi_c$  in PLA/HNT6 was slightly increased to 31.3% compared to that of PLA only that has 29.9%. According to Zhou and Xanthos,<sup>24</sup> the shifting of  $T_{cc}$  of PLA to lower temperature could be attributed to the nucleating effects of montmorillonite clay. Lower  $T_{cc}$  initiates faster crystallization.<sup>25</sup> The  $T_{cc}$  of PLA/HNT6 nanocomposites does not change much when the content of ENR was added. The addition of ENR in PLA nanocomposites showed increasing of  $\chi_c$  although the  $\chi_c$  value of PLA/HNT/ENR is still lower than PLA and PLA/HNT6 nanocomposites. The  $\chi_c$  of PLA/HNT6/

ENR20 was slightly increased compared to PLA/HNT6 nanocomposites. Similar results were reported by Thongpin *et al.*<sup>26</sup> where the ENR and organo-montmorillonite (OMMT) could act as nucleating agents, resulting in the increase of crystallinity of PLA. The addition of 5 wt % ENR in PLA/HNT6 nanocomposites gives the lower  $\chi_c$  value as ~16.5% and increases again when the loading of ENR increases. Besides, the PLA/HNT6/ENR5 nanocomposites had a single melting temperature of 152.3°C. It can be explained that in PLA/HNT6/ENR5, a strong interaction may occur between oxirane group of ENR and hydroxyl group of HNT, which provides good dispersion of HNT in PLA matrix, as a result, reduces the nucleation effect of HNT in PLA/HNT6/ENR5. According to Di *et al.*,<sup>27</sup> organoclay can act as nucleating agents. However, it can become a retardant of crystallization acting because of the strong interaction

**Figure 3.** FTIR spectra of HNT, PLA, and PLA/HNT6 nanocomposites.

**Table IV.** FTIR Spectra and its Assignment of PLA

| Wavenumber (cm <sup>-1</sup> ) | Assignment      |
|--------------------------------|-----------------|
| 1185, 1132, 1094–1087, 1045    | C—O—C group     |
| 869, 756                       | C—C stretching  |
| 1458, 1386, and 1362           | C—H deformation |
| 1760                           | C=O group       |
| 2998                           | C—H stretching  |
| 3500                           | O—H group       |

between polymer matrix and organoclay. The polymer chains that interacted with the nanoclay might partially immobilize and hinder the crystallization process.

#### Fourier Transform Infrared Spectroscopy Analysis (FTIR)

Figure 3 shows the FTIR spectra of HNT, PLA, and PLA/HNT6 nanocomposites. The characteristic functional groups of PLA, which commonly appear in 4000–400 cm<sup>-1</sup> region in the FTIR spectra are summarised in Table IV. It can be seen that new peaks at 3696, 3651, 3624, 912, 536, and 470 cm<sup>-1</sup> were detected in PLA/HNT6 spectra. The weak peak at 3651 cm<sup>-1</sup> can be revealed to the interaction of alkenes (C—H) with bridging framework OH groups and the external silanols group (Si—OH), respectively.<sup>28</sup> The end hydroxyl group of PLA could interact with silanol group of HNT. As a result, the C—H group from PLA could connect with the silanol group. The small peaks at 3696 and 3624 cm<sup>-1</sup> are assigned to the inner hydroxyl group (crystal water), which exists in clay minerals.<sup>29,30</sup> The weak band at 912 cm<sup>-1</sup> belonged to the inner OH group of Al—OH of the clay.<sup>31,32</sup> The band at 538 cm<sup>-1</sup> corresponded to Si—O—Al (octahedral Al), while the peak at 476 cm<sup>-1</sup> was attributed to Si—O—Si bending vibrations.<sup>33</sup> The spectrum of HNT shows the intensity band at 1030 cm<sup>-1</sup> assigned to the Si—O stretching vibrations.

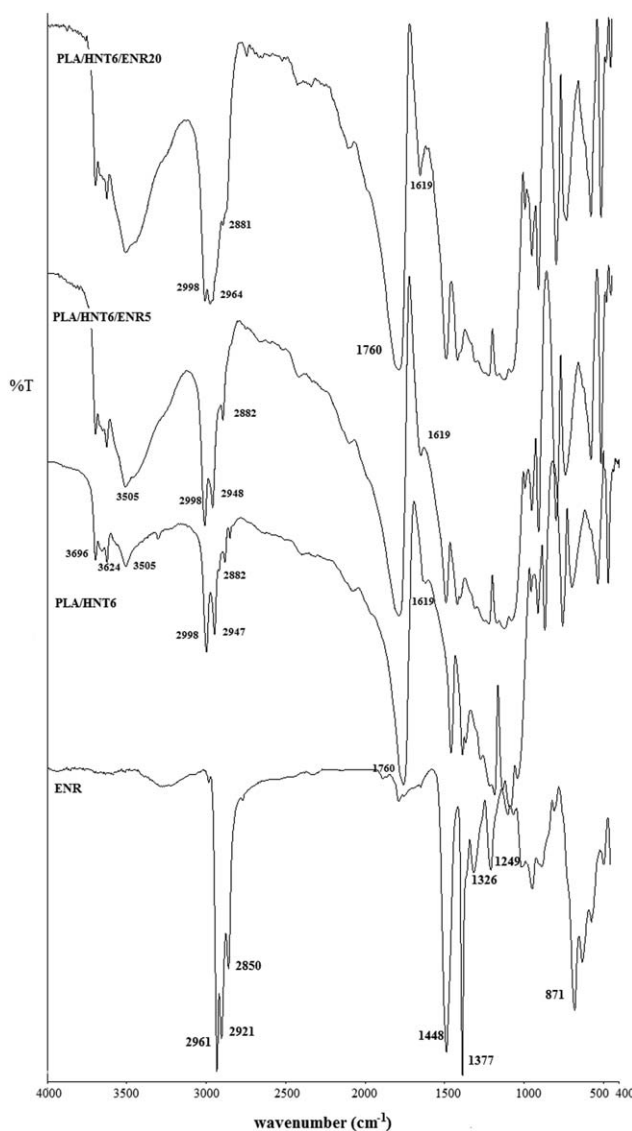
Figure 4 shows the FTIR spectra of ENR, PLA/HNT6, PLA/HNT6 with ENR loading. From the FTIR spectra of ENR, the peaks at 2961, 2921, and 2858 cm<sup>-1</sup> are originated from C—H stretching from —CH<sub>2</sub> group. The absorption bands at 1448 and 1377 cm<sup>-1</sup> are attributed to the C—H stretching from —CH<sub>3</sub> group. The peaks of 1326, 1249, and 871 cm<sup>-1</sup> can be assigned to the C—O stretching of oxiranes group in ENR. The stretching of C—H bonds leads to high absorption at 2998 and 2964 cm<sup>-1</sup> with a shoulder at 2881 cm<sup>-1</sup> are observed in FTIR spectra of PLA/HNT6/ENR20. The C—H stretching at the peak of 2964 cm<sup>-1</sup> was attributed to —CH<sub>3</sub> group of ENR as the ENR content increased. The peak at 1619 cm<sup>-1</sup> shifted to 1624 cm<sup>-1</sup> corresponding to C=O stretching. The intensity band at 1624 cm<sup>-1</sup> become more obvious for PLA/HNT6/ENR20, which indicated that the interaction between the carboxylic end group of PLA chains and oxirane group of ENR had resulted in the formation of C—O group. The peak at 3505 cm<sup>-1</sup> shifted to 3487 cm<sup>-1</sup>, which can be assigned to O—H stretching. The intensity peak at 3487 cm<sup>-1</sup> increased, which is caused by O—H stretching produced at the oxirane group of ENR when esterification reaction occurs between PLA and ENR. Figure 5(a) shows the proposed interaction between PLA and ENR. Also, the OH group of HNT may interact with

oxirane group of ENR and carbonyl group of PLA with the formation of hydrogen bonding as shown in Figure 5(b).

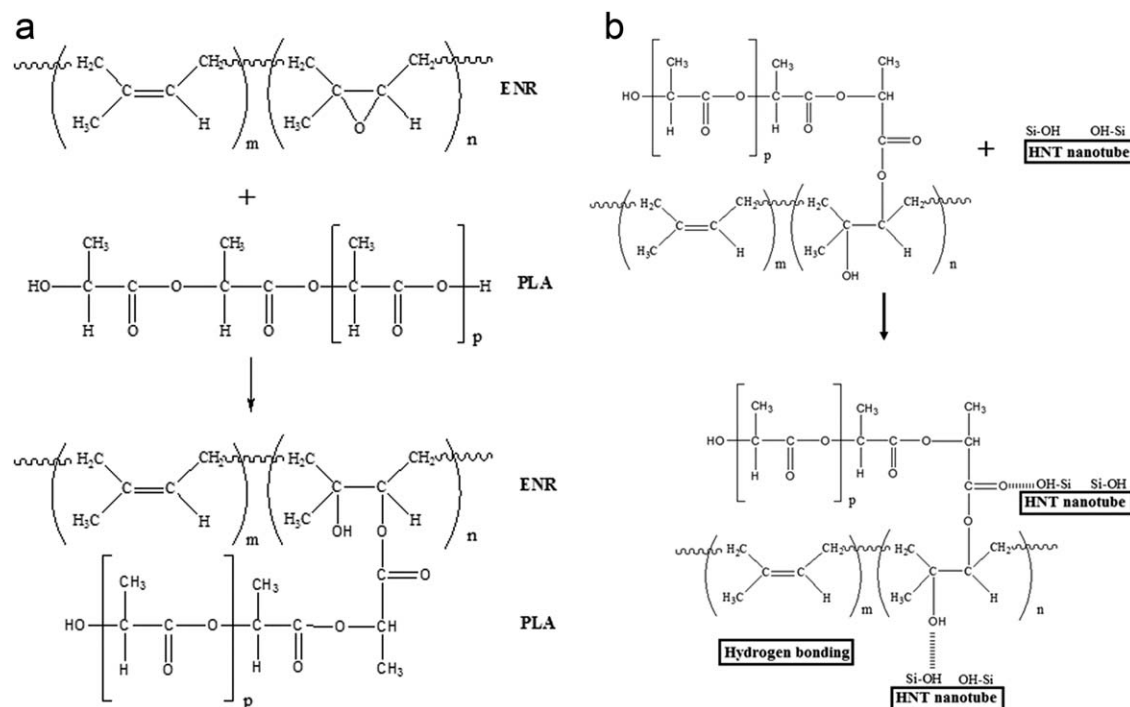
#### Field Emission Scanning Electron Microscopy (FESEM)

Figure 6 shows FESEM micrographs taken from impact fracture surfaces of PLA nanocomposites. The fracture surface of PLA [c.f., Figure 6(a)] showed relatively smooth flaw with a small number of crazes causing the premature rupture of the specimens, which indicates typical brittle fracture surface. In contrast, the formation of nonplanar fracture surfaces and plastic deformation in PLA/HNT6 can be observed in Figure 6(b). A relatively rough fracture surface and crack fronts on the fracture surface of PLA/HNT6 was investigated. It was suggested that a crack path deflection due to the rigidity of HNT nanotube hindered crack propagation, which the energy dissipated during the fracture mechanism.<sup>34</sup> Therefore, HNT could improve impact strength of PLA.

Figure 6(c) shows a rather rough fracture surface and parabolic marking derived from primary and secondary crack fronts



**Figure 4.** FTIR spectra of PLA/HNT6, PLA/HNT6/ENR5, and PLA/HNT6/ENR20.



**Figure 5.** (a) Proposed interactions between PLA and ENR. (b) Proposed interactions between PLA, ENR, and HNT.

travelling in one craze zone were investigated, respectively. During the crack propagation, a certain molecular coil size is necessary to allow the transfer of stresses sufficient for the initiation

and temporary propagation of a secondary fracture plane. In other words, the appearance of parabolic markings on the fracture surface is correlated with the energy consumed during

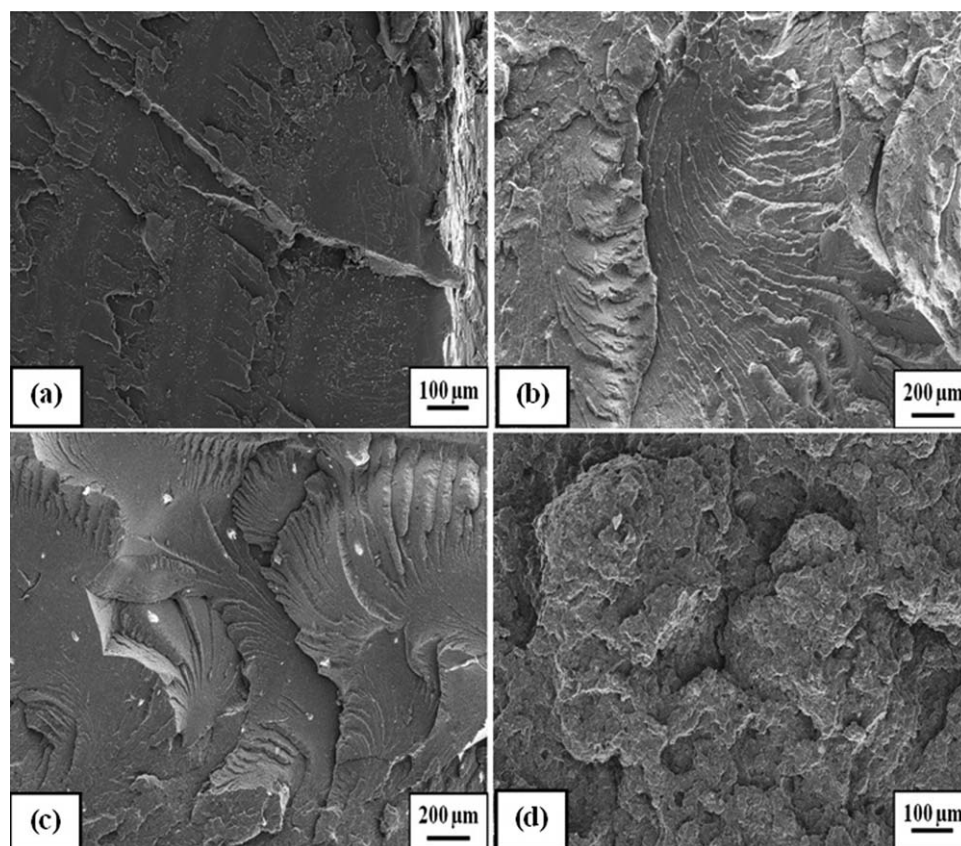


**Figure 6.** FESEM micrographs taken from impact fracture surfaces of (a) PLA, (b) PLA/HNT6, (c) PLA/HNT6/ENR5, and (d) PLA/HNT6/ENR15.

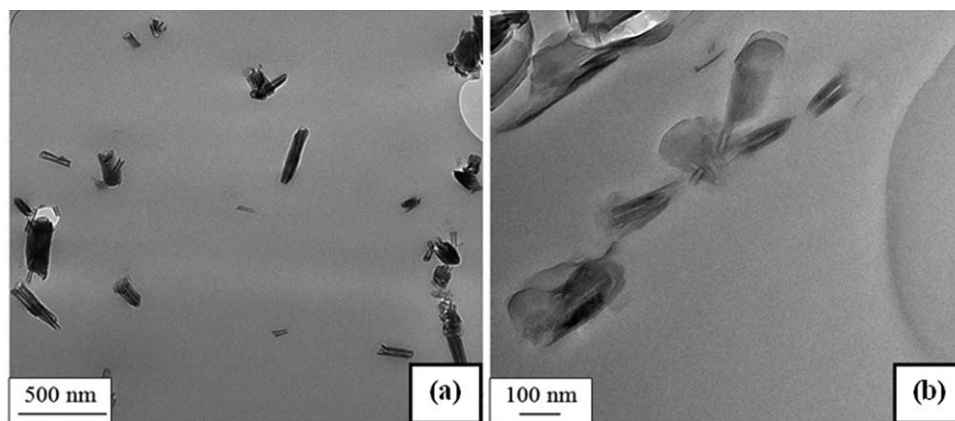


**Figure 7.** TEM images of (a) PLA/HNT6 and (b) PLA/HNT6/ENR20.

applied impact energy.<sup>35</sup> The increase of impact strength in PLA/HNT6/ENR5 was suggested the dissipated energy during the fracture mechanism. A more extensive of plastic deformation and rougher surface were observed on the fracture surface of PLA/HNT6 that constituted of 15 wt % ENR as shown in Figure 6(d). The crazing is commonly controlled by the foreign particles, which act as stress concentrators. The rubber-modified polymer acts as stress concentrators due to the formation of a large number of crazes distributed throughout the sample volumes. The mechanism of craze initiation include rubber particles cavitation, crazing within the rubber particles, and crazing in the matrix phases<sup>36</sup> to form uneven fractures surface on the PLA/HNT6/ENR15 nanocomposites in relation to the total dissipated energy. Higher impact strength of PLA/HNT6/ENR15 nanocomposites owing to the fact that energy dissipated during the creation of the new fracture surface on the applied impact energy.

#### Transmission Electron Microscopy (TEM)

Figure 7 shows the TEM micrographs of the PLA/HNT6 and PLA/HNT6/ENR20 nanocomposites. It can be seen in Figure 7 that the HNT are dispersed in the PLA matrix with the length 0.5–1.2  $\mu\text{m}$  and the diameter was 50–100 nm. HNT has a hollow cylindrical shape and contains a transparent central area along the cylinder with an open-end. For the PLA nanocomposites containing 6 wt % of HNT, co-exist of nano-dispersed HNT and agglomerate HNT can be observed in the PLA matrix [c.f., Figure 7(a)]. TEM images of PLA/HNT6/ENR20 are

shown in Figure 7(b). The dark regions in the TEM images correspond to ENR particles with the dimension between 0.15 and 0.30  $\mu\text{m}$ . It can be observed that the HNT are located in the ENR particles surface. It is worth mentioning that the HNT has good affinity with the ENR chains. In Figure 7(b), the surface of HNT has a tendency to form “bridge-like” formations with each other at the interface between ENR and PLA.

#### Water Absorption Tests

Table V summarises the percentage at maximum water absorption ( $M_m$ ) of PLA/HNT nanocomposites measured at immersion temperatures of 30, 40, and 50°C. The  $M_m$  values of the PLA/HNT6 are higher than that of unfilled PLA. It can be seen that the  $M_m$  of PLA/HNT6 nanocomposite are  $\sim 1.25\%$ , while the PLA is  $\sim 0.4\%$ . This indicates that the presence of abundant hydroxyl group in HNT tends to interact with water molecules. According to Yew *et al.*,<sup>37</sup> higher  $M_m$  value of the PLA composites was attributed to the hydrophilic nature of filler, which was available for interaction with water molecules. A dramatic increase of the  $M_m$  was observed with further increase of ENR content. It was due to the oxirane group of ENR, which tend to interact with water molecules, and thus, facilitate water penetration into polymer matrix. The  $M_m$  values of PLA and HNT-filled PLA (with and without ENR) at 40 and 50°C increased dramatically compared to the samples immersed at 30°C. This is due to the higher immersion temperature, where water molecules gain higher energy for the diffusion process. In other words, higher temperature increased the mobility of water

**Table V.** Maximum Water Absorption ( $M_m$ ), Diffusion Coefficient ( $D$ ), and Activation Energy of Water Diffusion ( $E_a$ ) of PLA/HNT Nanocomposites

| Material designation | Maximum water absorption, $M_m$ (%) |      |      | Diffusion coefficient, $D$ ( $\times 10^{-12}$ ) ( $\text{m}^2 \text{s}^{-1}$ ) |      |      | $E_a$ ( $\text{kJ mol}^{-1}$ ) |
|----------------------|-------------------------------------|------|------|---|------|------|--------------------------------|
|                      | 30°C                                | 40°C | 50°C | 30°C  | 40°C | 50°C |                                |
| PLA                  | 0.40                                | 0.91 | 1.86 | 2.79  | 2.92 | 3.04 | 3.50                           |
| PLA/HNT6             | 1.25                                | 3.00 | 4.11 | 0.81  | 1.21 | 1.68 | 29.72                          |
| PLA/HNT6/ENR5        | 1.76                                | 4.26 | 6.46 | 0.97  | 1.38 | 2.11 | 31.60                          |
| PLA/HNT6/ENR10       | 2.14                                | 4.79 | 6.60 | 0.86  | 1.35 | 1.89 | 32.10                          |
| PLA/HNT6/ENR15       | 2.58                                | 5.43 | 7.20 | 0.85  | 1.21 | 1.86 | 31.84                          |
| PLA/HNT6/ENR20       | 3.07                                | 6.31 | 7.68 | 0.83  | 1.18 | 1.82 | 31.93                          |

molecules, providing fast access of water into polymer segments.<sup>38,39</sup>

Table V shows the diffusion coefficient ( $D$ ) and activation energy of water diffusion ( $E_a$ ) for PLA nanocomposites at immersion temperatures of 30, 40, and 50°C. The incorporation of 6 wt % HNT into the PLA matrix increased the tortuous path of the water diffusion through the specimen. The  $D$  values of PLA decreased with the incorporation of HNT and ENR. The loading of ENR in PLA/HNT nanocomposites showed a decrease in  $D$  values. This is due to the physical hindrance of ENR to the diffusion of water molecules.

The higher loading of HNT in PLA nanocomposites may also contribute in barrier effect to water transportation. The addition of ENR and HNT in PLA increases the transportation path of water molecules. The decrease of the  $D$  values for PLA/HNT/ENR may be due to the good interfacial adhesion between the oxirane group of ENR and HNT, and thus reduce the water accumulation in between the interphase of ENR and HNT.

The  $E_a$  is an energy barrier that a material has to overcome against diffusion of water.<sup>40</sup> The  $E_a$  values of PLA/HNT6 nanocomposites are higher than that of neat PLA, which the  $E_a$  value of PLA increased drastically from 3.5 to 29.7 kJ mol<sup>-1</sup> in PLA/HNT6 nanocomposites. The loading of ENR in PLA/HNT6 nanocomposites effectively increased the  $E_a$  values. It was suggested that the barrier contribution of HNT and the polarity site of ENR hindered water transportation. Accordingly, when the water bounded within the polarity site of the composite, the water molecules may accumulate in the interface of composites and form an extremely thin water layer surrounding HNT. These water molecules are much less mobile. Thus, it will restrict the rest of water molecules further and diffuse into the interface of PLA nanocomposites. Consequently, the water molecules need more energy to transport into the PLA nanocomposites.

## CONCLUSIONS

Based on this research, the effect of ENR on the mechanical, thermal, water absorption, and morphological properties of poly(lactic acid)/halloysite nanocomposites, can be concluded below:

The PLA/HNT6 nanocomposites contain 15 wt % ENR give the highest impact strength with an enhancement of about 296%. Higher impact strength of PLA/HNT6/ENR15 nanocomposites owing to the fact that energy dissipated during the creation of the new fracture surface on the applied impact energy which was evidenced by FESEM. The HNT has good affinity with PLA and ENR which was revealed by TEM and FTIR. The  $T_m$ ,  $T_{cc}$  and  $\chi_c$  of PLA/HNT6 nanocomposites were affected by the ENR content. The incorporation of HNT and ENR increase its nucleation effect and assist in the crystallization process of PLA. The addition of ENR in PLA/HNT6 nanocomposites exhibited higher  $M_w$  due to their functional group interaction with water. A reduction of diffusion coefficient ( $D$ ) of PLA was observed in the presence of HNT and ENR. The  $E_a$  values for PLA were increased by the addition of HNT and ENR.

## ACKNOWLEDGMENTS

This study was funded by Universiti Sains Malaysia Research University Grant (grant number 814070; grant number 814199) and Ministry of Higher Education Malaysia MyPHD Scholarship Programme.

## REFERENCES

1. Santiago, F.; Mucientes, F.; Osorio, A. E.; Rivera, M. C. *Eur. Polym. J.* **2007**, *43*, 1.
2. Garlotta, D. *J. Polym. Environ.* **2001**, *9*, 63.
3. Yu, L.; Dean, K.; Li, L. *Prog. Polym. Sci.* **2006**, *31*, 576.
4. Cai, Y. M.; Lv, J. G.; Feng, J. M. *J. Polym. Environ.* **2013**, *21*, 108.
5. Wang, Y. L.; Hu, X.; Li, H.; Ji, X.; Li, Z. M. *Polym. Plast. Technol. Eng.* **2010**, *49*, 1241.
6. Zeng, J. B.; Li, Y. D.; Zhu, Q. Y.; Yang, K. K.; Wang, X. L.; Wang, Y. Z. *Polymer.* **2009**, *50*, 1178.
7. Tham, W. L.; Poh, B. T.; Mohd Ishak, Z. A.; Chow, W. S. *J. Therm. Anal. Calorim.* **2014**, *118*, 1639.
8. Zhang, L.; Li, C.; Huang, R. *J. Polym. Sci. B: Polym. Phys.* **2005**, *43*, 1113.
9. Tham, W. L.; Mohd Ishak, Z. A.; Chow, W. S. *J. Macromol. Sci. B: Phys.* **2014**, *53*, 371.
10. Zakaria, Z.; Islam, M. S.; Hassan, A.; Mohamad Haafiz, M.; Arjmandi, R.; Inuwa, I.; Hasan, M. *Adv. Mater. Sci. Eng.* **2013**, *2013*, Article ID 629092.
11. Rajasekar, R.; Pal, K.; Heinrich, G.; Das, A.; Das, C. *Mater. Des.* **2009**, *30*, 3839.
12. Pongtanayut, K.; Thongpin, C.; Santawitee, O. *Energy Proc.* **2013**, *34*, 888.
13. Noriman, N.; Ismail, H.; Rashid, A. *Polym. Test.* **2010**, *29*, 200.
14. Ismail, H.; Ooi, Z. X. *Polym. Plast. Technol. Eng.* **2010**, *49*, 688.
15. Wang, H.; Sun, X.; Seib, P. *J. Appl. Polym. Sci.* **2001**, *82*, 1761.
16. Zuiderduin, W.; Westzaan, C.; Huetink, J.; Gaymans, R. *Polymer* **2003**, *44*, 261.
17. Lin, Y.; Ng, K. M.; Chan, C. M.; Sun, G.; Wu, J. *J. Colloid Interface Sci.* **2011**, *358*, 423.
18. Bartczak, Z.; Argon, A. S.; Cohen, R. E.; Weinberg, M. *Polymer* **1999**, *40*, 2347.
19. Barrientos-Ramírez, S.; Ramos-Fernández, E.; Silvestre-Albero, J.; Sepúlveda-Escribano, A.; Bartczak, Z.; Argon, A. S.; Cohen, R. E.; Weinberg, M. *Microporous Mesoporous Mater.* **2009**, *120*, 132.
20. Sarasua, J. R.; Prud'homme, R. E.; Wisniewski, M.; Borgne, A. L.; Spassky, N. *Macromolecules* **1998**, *31*, 3895.
21. Chow, W. S.; Lok, S. K. *J. Thermoplast. Compos. Mater.* **2008**, *21*, 265.
22. Goffin, A. L.; Raquez, J. M.; Duquesne, E.; Siqueira, G.; Habibi, Y.; Dufresne, A.; Dubois, P. *Biomacromolecules* **2011**, *12*, 2456.



23. He, Y.; Fan, Z.; Wei, J.; Li, S. *Polym. Eng. Sci.* **2006**, *46*, 1583.
24. Zhou, Q.; Xanthos, M. *Polym. Degrad. Stab.* **2009**, *94*, 327.
25. Zhang, Y.; Deng, B.; Liu, Q.; Chang, G. *J. Macromol. Sci. B Phys.* **2013**, *52*, 334.
26. Thongpin, C.; Kuttanate, N.; Kampuang, K.; Suwanwanit, N. *J. Met. Mater. Miner.* **2012**, *22*, 105.
27. Di, Y.; Iannace, S.; Maio, E. D.; Nicolais, L. *J. Polym. Sci. B: Polym. Phys.* **2005**, *43*, 689.
28. Su, B. L.; Jaumain, D. *Stud. Surf. Sci. Catal.* **2007**, *170*, 1283.
29. Frost, R.; Kristof, J.; Horvath, E.; Klopogge, J. *Clay Miner.* **2000**, *35*, 443.
30. Geng, W.; Nakajima, T.; Takanashi, H.; Ohki, A. *Fuel* **2009**, *88*, 139.
31. Agarwal, M.; Koelling, K. W.; Chalmers, J. J. *Biotechnol. Prog.* **1998**, *14*, 517.
32. Bocchini, S.; Fukushima, K.; Blasio, A. D.; Fina, A.; Frache, A.; Geobaldo, F. *Biomacromolecules* **2010**, *11*, 2919.
33. Madejová, J. *Vib. Spectrosc.* **2003**, *31*, 1.
34. Alhuthali, A.; Low, I. M. *J. Appl. Polym. Sci.* **2013**, *130*, 1716.
35. Kausch, H. H. *Polymer Fracture (Polymer, Properties and Applications 2)*; Springer-Verlag: Berlin, **1987**; p 305.
36. Henton, D. E.; Bubeck, R. A. In *Polymer Toughening*; Arends, C. B., Ed.; Marcel Dekker: New York, **1996**; p 237.
37. Yew, G.; Mohd Yusof, A.; Mohd Ishak, Z. A.; Ishiaku, U. *Polym. Degrad. Stab.* **2005**, *90*, 488.
38. Karaduman, Y.; Onal, L. *J. Compos. Mater.* **2011**, *45*, 1559.
39. Srubar, W. V.; Frank, C. W.; Billington, S. L. *Polymer* **2012**, *53*, 2152.
40. Muthirakkal, S.; Narasimha Murthy, H. N. R.; Krishna, M.; Rai, K. S.; Karippal, J. J. *Iran. Polym. J.* **2010**, *19*, 89.